3D networks containing rectangular Sr_4 and Ba_4 units: Synthesis, structure, bonding and potential application for Ne gas separation

Subhajit Mandal[1], Sudip Pan[1], Dibakar Deb[1], Santanab Giri[1], Soma Duley[1], Slavko Radenković[2], David L. Cooper[3], Patrick Bultinck[4], Anakuthil Anoop[1], Manish Bhattacharjee[1,*] and Pratim K. Chattaraj[1,*]

[1] *Department of Chemistry, Indian Institute of Technology, Kharagpur 721302, India.*
[2] *Faculty of Science, University of Kragujevac, P.O. Box 60, 34000 Kragujevac, Serbia.*
[3] *Department of Chemistry, University of Liverpool, Liverpool L69 7ZD, United Kingdom.*
[4] *Department of Inorganic and Physical chemistry of Ghent University, Krijgslaan 281 (S3), B-9000 Gent, Belgium.*

*E-mails for the corresponding authors: manishbhattacharjee06@gmail.com; pkc@chem.iitkgp.ernet.in

Abstract

New porous 3D metal-organic frameworks are synthesized that contain infinite chains of Sr_n and Ba_n rectangles. Their structures are elucidated by means of spectroscopic techniques such as NMR and IR, and the respective crystal structures are determined. The electronic structure of basic units of the crystals are computed using density functional theory at the B3LYP/6-31G(d,p)/def2-TZVP level of theory and the bonding and reactivity are analyzed using natural bond orbital analysis, the quantum theory of atoms in molecules and conceptual density functional theory. The possibilities of noble gas storage inside the crystal structures are explored through the free optimization of the noble gas atom containing crystal, keeping frozen the geometries of the units derived from the crystal structure. It was found that a neon atom can fit into a cavity in the Sr and Ba crystal structures whereas other noble gases (He, Ar, Kr) exhibit repulsive interaction with the crystal structure. *Ab initio* molecular dynamics simulations for up to 500 fs at 77 K and 298 K suggest that the structures incorporating a neon atom are kinetically stable.

Keywords: Metal-organic framework, Natural bond orbital analysis, Reactivity descriptors, Electron density analysis, Noble gas storage.

1. Introduction

Metal-organic frameworks (MOFs) are molecular structures based on metal ions coordinated to organic ligands[1-3] which can act as porous hosts.[4,5] Syntheses of 3D polymeric materials have received much attention in recent years.[6] This is mainly due to their potential use in gas absorption, gas separation, ion exchange and catalysis. These framework materials typically have very low density and very high surface area, which can make them ideal for gas absorption, storage and separation.[5,7-9] For example, MOFs have been widely used for gas chromatographic separation of alkenes[10] and they have also been shown to be effective in the absorption of harmful gases such as SO_2, NH_3, Cl_2 and CO.[11] One of the major interests in this field is the syntheses of MOFs for hydrogen storage.[5-8] It may be noted that it is mainly transition metals including zinc and cadmium complexes that have been used so far for the formation of MOFs, whereas there have been relatively few studies of porous networks based on group 1 or group 2 elements.[12] We report here, the synthesis and structure determination of $[M(NTA\text{-}H)(H_2O)_{1.5}]_n$ MOFs in which M is Sr (**1a**) or Ba (**1b**), and NTA and NTA-H are nitrilotriacetate and N-protonated nitrilotriacetate, respectively (see scheme 1).

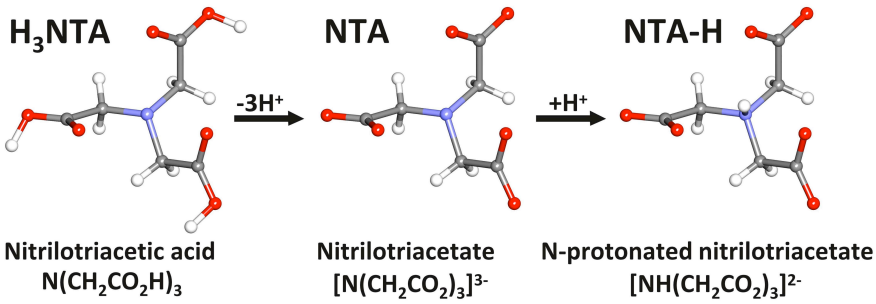

Scheme **1**

Ma and Zhou[13] have studied a number of porous MOFs, which are suitable for H_2, CO_2 and CH_4 storage. We find that the spacing between two acetate ligands in **1a** and **1b** is close to 3 Å, which could be large enough to enclose noble gas atoms, but it is not sufficient for storing molecules.

In the recent years, many noble gas (Ng) compounds have either been detected experimentally[14-18] or have been predicted to be stable theoretically[19-23] despite their inertness. The encapsulation of Ng atoms inside a cage like fullerene and other smaller cages has also been investigated theoretically as well as experimentally.[24,25] However, the number of experimental and/or theoretical studies on Ng storage with

MOFs is small. In computational studies, Greathouse *et al.*[26] have shown selective absorption of Xe and Ar from air by some specific MOFs. Ryan and coworkers[27] have shown computationally that MOFs can be promising materials for the separation of Xe and Keskin *et al.*[28] have studied various MOFs for Xe/Kr and Xe/Ar separations.

In the present work, we assess the bonding pattern and reactivity of the crystal structures **1a** and **1b** by means of natural bond orbital (NBO) analysis, the quantum theory of atoms in molecules (QTAIM) and the use of various descriptors based on conceptual density functional theory (CDFT). Subsequently, the MOFs, **1a** and **1b,** are examined as potential storage materials for Ng atoms; specifically He, Ne, Ar and Kr. *Ab initio* molecular dynamics simulation are used to assess the kinetic stability of Ng atoms inside **1a** and **1b**.

2. Experimental Section

The chemicals used were reagent grades products. The ^{1}H NMR spectrum was recorded on a Bruker Avance II spectrometer (400 MHz). Carbon, hydrogen and nitrogen analyses were performed using a Perkin Elmer 2400 series II analyzer. Infrared spectrum was recorded on a Perkin Elmer FT-IR Spectrometer (SPECTRUM *RXI*).

2.1. Syntheses of $[Sr(NTA\text{-}H)(H_2O)_{1.5}]_n$ (1a) and $[Ba(NTA\text{-}H)(H_2O)_{1.5}]_n$ (1b) {NTA-H = N - protonated nitrilotriacetate }

Nitrilotriacetic acid (H_3NTA) (0.91 g, 1 mmol) was added to an aqueous solution of NaOH (0.08 g, 2 mmol) and the mixture was stirred for 15 mins. The resulting solution was filtered and to this $SrCl_2.6H_2O$ (1.066 g, 4 mmol) was added and the solution was refluxed for 3 hrs. The solution pH at this stage was found to be 1. The solution was filtered and allowed to stand for a week, whereupon colorless crystals of $[Sr(NTA\text{-}H)(H_2O)_{1.5}]_n$ appeared. The same procedure was used for the synthesis of compound **1b**, using barium chloride dihydrate (0.976 g, 4 mmol). **1a**: Yield: 87% (0.263 g). Anal calcd. for $C_6H_{10}NO_{7.5}Sr$ (mol wt. = 303.77): C; 23.72; H: 3.32; N: 4.61. Found: C: 23.90; H: 3.02; N: 4.84. IR (cm^{-1}): 2985, 1665, 1630, 1395. **1b**: Yield: 84% (0.297 g). Anal calcd. for $C_6H_{10}NO_{7.5}Ba$ (mol wt. = 353.475): C; 20.52; H: 2.72; N: 4.01. Found: C: 20.39; H: 2.85; N: 3.96. IR (cm^{-1}): 2988, 1660, 1632, 1391.

2.2. Crystal structure determination

Suitable crystals of $[Sr(NTA\text{-}H)(H_2O)_{1.5}]_n$ (**1a**) and $[Ba(NTA\text{-}H)(H_2O)_{1.5}]_n$ (**1b**) were grown from water over a period of five to seven days at room temperature.[29] The single crystal data were collected on a Bruker Smart APEX system that uses molybdenum Kα radiation (λ = 0.71073 Å). No absorption correction was used. The structure was solved by direct method and refined by least square method on F^2 employing WinGx package[30] and the relevant programs (SHELXS[31] and SHELXL[31] and ORTEP[32] for windows) implemented therein. Non hydrogen atoms were refined anisotropically and hydrogen atoms on carbon atoms and nitrogen atoms could be located in Fourier difference map and refined by mixed method.

3. Theoretical study

The molecular structures of Sr and Ba crystals were extracted from the experimental crystallographic data presented in this article.[29] Single point computations were carried out on the simplified models of the extended crystal structures (**2a**, **2b**, **3a** and **3b** in supporting information) without geometry optimization to better reflect the characteristics of **1a** and **1b**. All single point calculations were done using Gaussian 09 program package.[33] The B3LYP[34] functional was used for single point calculations employing 6-31G(d,p)[35] basis set for C, N, O and H atoms and def2-TZVP[36] basis set with corresponding quasi-relativistic pseudopotentials[37] for Sr and Ba atoms. Natural bond orbital (NBO)[38] analysis was performed at the same level of theory as implemented in Gaussian 09. Electron density analysis was done with Multiwfn software package.[39] For electron density analysis the wave functions were generated at B3LYP/6-31G(d,p)/def2-TZVP level of theory using Gaussian 09. CDFT based reactivity descriptors are employed to analyze the stability and reactivity of these clusters. Several electronic properties like ionization potential (IP), electron affinity (EA), electronegativity (χ),[40] hardness (η)[41] and electrophilicity (ω)[42] were calculated for these systems using the Koopmans' theorem[43] as follows:

$$IP = -E_{HOMO} \quad (1)$$

$$EA = -E_{LUMO} \quad (2)$$

where E_{HOMO} and E_{LUMO} are energies of the highest occupied molecular orbital (HOMO) and the lowest unoccupied molecular orbital (LUMO), respectively.

$$\eta = (IP - EA) \quad (3)$$

$$\chi = (IP + EA)/2 \quad (4)$$

$$\omega = \chi^2/2\eta \quad (5)$$

To understand the Ng adsorption capability of the studied crystals, Ng atom was placed inside the framework and optimized, keeping the framework frozen. The optimizations were performed in Turbomole 6.5 software package[44] using B3LYP functional employing def2-SVP[45] basis set and the corresponding auxiliary basis set for all the atoms. For Sr and Ba the effective core potentials[37] were taken into account for all the related structures. Empirical dispersion correction (D3)[46] with BJ dumping[47] was included in all optimization. Restricted approach was used in the computational analysis for the closed shell structures. The dynamics of the **Ne@3a** and **Ne@3b** systems were evaluated using *ab initio* molecular dynamics, atom-centered density matrix propagation (ADMP)[48] technique as implemented in Gaussian 09. The dynamics were studied at the B3LYP-D/LanL2DZ level with the above mentioned geometries. Boltzmann distribution was used to generate the initial nuclear kinetic energies of the systems. The temperature was maintained by using a velocity scaling thermostat throughout the simulation. For each of the system, simulation was carried out separately at 298 K and 77 K. Default random number generator seed was used, as implemented in Gaussian 09 to initiate the initial mass weighted Cartesian velocity. For all the cases, trajectories up to 500 fs were generated.

4. Results and discussion

The complexes are synthesized by a reaction of $SrCl_2 \cdot 6H_2O$ or $BaCl_2 \cdot 2H_2O$ and monosodium salt of nitrilotriacetic acid (**$Na[H_2NTA]$**) in water, in high yield. The compounds are characterized by elemental analyses and spectroscopic studies as well as single crystal X-ray diffraction studies. The elemental analyses agree well with the composition. FT-IR spectrum of the compound shows a strong band at 1630 cm^{-1} which is characteristic C=O stretching frequency and observed strong bands at 1665 and 1395 cm^{-1} characteristic of coordinated COO^- stretching frequencies. In addition, a band at 2986 arises for N-H stretching.

4.1. Crystal structure

Since the complexes, $[Sr(NTA\text{-}H)(H_2O)_{1.5}]_n$ (**1a**) and $[Ba(NTA\text{-}H)(H_2O)_{1.5}]_n$ (**1b**) are isostructural, only the details of the structural features of $[Sr(NTA\text{-}H)(H_2O)_{1.5}]_n$ have been described. The ORTEP drawing of the asymmetric unit of **1a** and **1b** is shown in Figures 1a and 1b.

The complex crystallizes in monoclinic space group C2/c. The asymmetric unit of $[Sr(NTA\text{-}H)(H_2O)_{1.5}]_n$ consists of one strontium atom coordinated to one oxygen, O1, of NTA-H ligand and two water oxygens O1W with full occupancy and O2W, with half occupancy (Figure 1a).

In the full structure, the strontium ion is nine coordinated and is coordinated to five NTA-H ligands and two water oxygens. Two carboxylate groups of two different NTA-H ligands bind the strontium center in a bidentate fashion through O1 and O2 of one ligand and O5 and O6 of another ligand. The other three carboxylate groups of NTA-H ligands bind the metal center in a monodentate fashion via O3, O4 and O7. In addition, the strontium center is coordinated to two water oxygens, O1W and O2W (Figure 2). Each NTA-H ligand binds five strontium atoms through five bridging carboxylate oxygens, O1, O2, O4, O5 and O6, out of which O1 and O6 bind two strontium ions in a μ_2 fashion (Figure 3). Thus, in solid state the complex forms a polymeric compound. Previously, Barnett *et al.*[49] described similar infinite network in Na(CaNTA) where $(CaNTA)^-$ units are linked together by the Na^+ ions and a formal charge on Ca in the complex is assumed to be close to +2. Lu *et al.*[50] reported 3D coordination polymers having molecular formulas $Na_3[Cu_2(NTA)_2(4,4'\text{-}bpy)]ClO_4.5H_2O$ and $[Cu_2(NTA)(4,4'\text{-}bpy)_2]ClO_4.4H_2O$. In **1a**, each O1 oxygen binds two strontium centers whereas two carboxylate oxygens, O6, from two ligands bind two strontium atoms in μ_2 fashion. Similarly, the water oxygen, O2W is bonded to two strontium atoms in a μ_2 fashion. Thus, four Sr atoms form a rectangular ring of Sr_4 units as evidenced by the observed ∠Sr1−Sr1− Sr1 angle, which is exactly 90° (Figure 4). The rectangular Sr_4 units are planar like cyclobutadiene as evidenced by the observed successive torsion angles, which were found to be zero (0) degree. In the Sr_4 rectangular unit, one of the observed Sr–Sr distances is 4.022 Å and another Sr–Sr distance is 5.056 Å.

In solid state, each strontium atom forms a node joining four strontium ions and forms a 3D polymeric network extending along crystallographic *a*, *b* and *c* axes (Figure 5). The most interesting feature of the network is the formation of infinite 1D chain of planar rectangular Sr_4 units. The polymeric Sr_4 network is planar as evidenced by the observed angles between three adjacent Sr atoms in the chain are 180 degree. This 1D chain grows along crystallographic *b* axis. There are three types of channels having average diameters, 7.5 Å, 6.6 Å and 6.3 Å.

4.2. Bonding

The crystal structures show that each metal site is coordinated with five NTA-H ligands and two water molecules. These are shown in structures, **2a** (having Sr as the metal) and **2b** (having Ba as the metal). Both **2a** and **2b** have four Sr and Ba atoms, respectively, six water molecules and fourteen NTA-H ligands (Figures 6a and 6b). The surface charges of the two acetate units originated from each NTA-H are passivated by adding hydrogen atoms. To understand the bonding pattern on the local sites of each metal atom, we have prepared two more structures **3a** and **3b**. In **3a** (containing Sr, shown in Figure 7a) and **3b** (containing Ba, shown in Figure 7b), each metal atom is surrounded by two water molecules and five NTA-H ligands. The surface charges are passivated by hydrogen atoms both in **3a** and **3b**.

4.2.1. NBO Analysis

Natural Population Analysis (NPA) shows that in the structure **2a**, Sr atoms have the natural charges as 1.05, 1.07, 1.08 and 0.93 |e|. Therefore, the average natural charge on each Sr atom is 1.03 |e|. The oxygen atoms of η^2 coordinated acetate units have -0.73, -0.73, -0.72 and -0.72 |e| natural charges for each Sr atom. The Wiberg bond indices (WBI)[51] for these Sr-O bonds are 0.15, 0.11, 0.14 and 0.10. The other oxygen atoms, which are directly coordinated to Sr atoms have the natural charges as -0.73, -0.73, -0.70 |e|. These Sr-O bonds show WBI values of 0.22, 0.22 and 0.14. In **2a**, N atoms have the natural charges ranging from -0.36 to -0.38 |e|. The water oxygen atoms for each Sr atoms show -0.92 and -0.98 |e| natural charges. WBI for Sr-O (water) bonds are 0.15 and 0.11. Similar charge distribution and WBI values like **2a** are found in **3a**. In **3a**, the natural charge on Sr atom is 1.01 |e|. The oxygen atoms of η^2 coordinated acetate units show natural charges ranging from -0.68 to -

0.75 |e|. For these η^2 coordinated Sr-O bonds, WBI values are in the range of 0.14-0.17. The other oxygen atoms, which are coordinated to Sr atom, have the natural charges around -0.70 |e|. These Sr-O bonds show WBI values of 0.24, 0.23 and 0.22. Nitrogen atoms in **3a** have the natural charges around -0.37 |e|. The water oxygens demonstrate NPA charges -0.96 and -0.95 |e|. WBI for Sr-O (water) bonds are 0.17 and 0.16. Therefore, we can consider **3a** as a smaller representation of **2a**. In case of **2b** and **3b**, similar trend of WBI values and charge distribution are observed.

4.2.2. Reactivity Descriptors

We have compared the reactivity descriptors between **2a** and **3a** and between **2b** and **3b** (see Table 1).

Table 1. Electronic state (ES), ionization potential (IP), electron affinity (EA), hardness (η), electronegativity (χ) and electrophilicity index (ω) in eV of **2a**, **2b**, 3**a** and 3**b** structures.

System	ES	IP	EA	η	χ	ω
2a	^{1}A	1.752	1.491	0.261	1.622	5.040
2b	^{1}A	1.204	0.949	0.255	1.077	2.273
3a	^{1}A	1.889	1.641	0.248	1.765	6.270
3b	^{1}A	1.214	0.913	0.301	1.064	1.881

Inspection of the reactivity descriptors reveals that the values are almost similar for **2a** and **3a**. The same trend is found between **2b** and **3b**. All these geometries are in ^{1}A electronic state. The IP and EA values have very small change between **2a** and **3a**, and also in between **2b** and **3b**. Similarly, the other reactivity parameters are almost similar. Therefore, we can consider the **3a** and **3b** as the smaller representation of **2a** and **2b**, respectively, where all the signatures for reactivity and bonding patterns are preserved.

4.2.3. Electron Density Analysis

An idea about the nature of bonding in **3a** and **3b** can be obtained from the analysis of the electron density. In AIM[52] formalism, the authentication of bonding is through the existence of a bond path between two atoms and a bond-critical point (BCP) associated with the path. The topological parameters obtained at the bond critical point (BCP) in between Sr-O and Ba-O bonds are provided in Table 2.

Negative value of Laplacian of electron density ($\nabla^2\rho(r_c)$) at the BCP indicates the accumulation of electron density, whereas positive value indicates electron density depletion at the BCP.[52] Hence, a negative value of $\nabla^2\rho(r_c)$ represents covalent interaction and a positive value describes non-covalent interaction. Thus, all the Sr-O bonds in 3**a** and Ba-O bonds in **3b** are of non-covalent type as per this analysis, because $\nabla^2\rho(r_c)$ are positive in all the BCPs. Low electron density ($\rho(r_c)$) also indicates the non-covalent nature. However, Macchi *et al.* have argued that for the systems comprising heavy atoms, $\nabla^2\rho(r_c)$ is not an efficient descriptor on its own.[53] There are also many failures of $\nabla^2\rho(r_c)$ to describe correctly a bond involving even lighter atoms.[54,55] Therefore, other parameters like kinetic energy density ($G(r_c)$), potential energy density ($V(r_c)$), electron energy density ($H(r_c)$) and the ratios - $G(r_c)/V(r_c)$ and $G(r_c)/\rho(r_c)$ are also calculated to get further insight into the bonding nature in **3a** and **3b**. Cremer *et al.*[56] suggested that if $\nabla^2\rho(r_c) > 0$ and $H(r_c) < 0$, the bonding is partially of covalent type whereas $H(r_c) > 0$ can be an indication of non-covalent bonding. Further, if the value of $-G(r_c)/V(r_c)$ remains in between 0.5 and 1 then there exists some degree of covalent character (partial covalent character).[57] The ratio of $G(r_c)/\rho(r_c)$ is also employed as an indicator of covalent bond.[53, 58, 59] Generally the value of $G(r_c)/\rho(r_c)$ less than 1 indicates the presence of covalent bonding and more than 1 suggests non-covalent interactions. In case of **3a** and **3b** the Sr-O and Ba-O bonds show $G(r_c)/\rho(r_c)$ values close to 1 and $-G(r_c)/V(r_c)$ value is more than 1. Hence these Sr-O bonds in **3a** and Ba-O bonds in **3b** show non-covalent bonding induced by electrostatic interactions.

Table 2. Electron density descriptors (au) at the bond critical points (BCP) in the coordination sphere of **3a** and **3b** obtained from the wave functions generated at B3LYP/6-31G(d,p)/def2-TZVP level of theory.

BCP	$\rho(r_c)$	$\nabla^2\rho(r_c)$	$G(r_c)$	$V(r_c)$	$H(r_c)$	$-G(r_c)/V(r_c)$	$G(r_c)/\rho(r_c)$
Sr-O (Water)	0.0263	0.1175	0.0262	-0.0230	0.0032	1.1374	0.9964
Sr-O (Water)	0.0272	0.1292	0.0282	-0.0241	0.0041	1.1705	1.0344
Sr-O (η^2)	0.0138	0.0553	0.0124	-0.0109	0.0015	1.1356	0.8971
Sr-O (η^2)	0.0267	0.1114	0.0253	-0.0228	0.0025	1.1108	0.9481
Sr-O (η^2)	0.0196	0.0775	0.0176	-0.0158	0.0018	1.1130	0.8973
Sr-O (η^2)	0.0215	0.0843	0.0192	-0.0173	0.0019	1.1104	0.8918
Sr-O (M-O)	0.0258	0.1087	0.0243	-0.0214	0.0029	1.1338	0.9420
Sr-O (M-O)	0.0266	0.1235	0.0270	-0.0231	0.0039	1.1693	1.0129
Sr-O (M-O)	0.0257	0.1156	0.0254	-0.0220	0.0035	1.1572	0.9888

Ba-O (Water)	0.0355	0.1230	0.0317	-0.0327	-0.0010	0.9697	0.8932
Ba-O (Water)	0.0362	0.1274	0.0325	-0.0331	-0.0062	0.9813	0.8962
Ba-O (η^2)	0.0224	0.0785	0.0179	-0.0162	0.0017	1.1043	0.7996
Ba-O (η^2)	0.0192	0.0674	0.0154	-0.0140	0.0014	1.0997	0.8057
Ba-O (η^2)	0.0193	0.0684	0.0157	-0.0143	0.0014	1.0961	0.8137
Ba-O (η^2)	0.0257	0.0938	0.0217	-0.0199	0.0018	1.0891	0.8447
Ba-O (M-O)	0.0253	0.0946	0.0212	-0.0188	0.0024	1.1276	0.8405
Ba-O (M-O)	0.0268	0.1097	0.0243	-0.0212	0.0031	1.1470	0.9076
Ba-O (M-O)	0.0238	0.0926	0.0206	-0.0181	0.0025	1.1392	0.8668

5. Noble gas storage (He, Ne, Ar, Kr)

To identify the plausible storage of Ng inside the structures **3a** and **3b**, we have considered a particular pore inside the crystal as a case study and have analyzed the interaction energy (ΔE_{int}). The interaction energy is calculated following the equation,

$$\Delta E_{int} = E_{Ng@x} - (E_{Ng} + E_x) \qquad (x = \textbf{3a} \text{ or } \textbf{3b}) \qquad (6)$$

Negative value of ΔE_{int} indicates that the presence of Ng inside the crystal stabilizes the system. Hence, from Table 3 we can say that only Ne shows stabilizing interaction with **3a** and **3b**.

Table 3. Interaction energy (ΔE_{int}) in kcal/mol between the noble gas (Ng) and crystal structures calculated at the B3LYP-D3(BJ)/def2-SVP level of theory.

System	ΔE_{int}	System	ΔE_{int}	System	ΔE_{int}	System	ΔE_{int}
He@3a	1.8	**Ar@3a**	29.1	**He@3b**	0.4	**Ar@3b**	14.9
Ne@3a	-1.8	**Kr@3a**	57.0	**Ne@3b**	-5.4	**Kr@3b**	36.4

Helium shows small destabilizing interaction, whereas Ar and Kr show large destabilization on entrapment inside **3a** and **3b**. The size of pore seems to be responsible for this observation. The selective absorption of Ne atom further shows the applicability of these MOFs towards separation of Ne from a mixture of noble gases. It may also be noted that the pore is too small to entrap a diatomic molecule, even a H_2 molecule. Therefore, the present MOFs can also separate Ne from a mixture with other gases. Though previously some studies reported the selective absorption of heavier Ng atoms,[**Error! Bookmark not defined.** - **Error! Bookmark not defined.**] with best of our knowledge no study is made so far on selective Ne absorption. Hence, the present

systems may find their importance in industry also. It may be noted that since here we have only optimized the Ng atoms keeping the crystal units frozen, the thermal effects and entropy contributions are not taken into account.

To explore this result further we have performed *ab initio* molecular dynamics at 77 K and 298 K on **Ne@3a** and **Ne@3b** systems. The movies are supplied in the electronic supporting information file. Recent articles have shown that the gas storage capacity of cages and MOFs increases at 77 K.[60] Dynamics at 77 K show that in **Ne@3a**, the distance between Ne and Sr atoms becomes 4.001 Å at the end of the simulation, which is slightly more than the initial Ne-Sr distance of 3.900 Å. During the simulation Ne atom remains trapped in between three acetate units of **3a**. At 298 K simulation, after 500 fs the distance between Ne and Sr decreases to 3.240 Å, and the crystal structures become somewhat distorted. In case of **Ne@3b**, molecular dynamics simulation at 77 K reveals that Ne atom comes closer to the central Ba atom gradually with time of simulation (at 0 and 500 fs the Ne-Ba distances are 4.008 Å and 3.365 Å, respectively). At 298 K, after 500 fs the distance between Ne and Ba atoms becomes 3.254 Å. All the movies show that the Ne atoms are not going out of the crystal units, though distortions can be seen in some parts of the crystal units at higher temperatures. Evolution of reactivity descriptors with time is shown in Figure S1 (supporting information). These plots show that the values of η and χ gradually increase up to 200 fs and thereafter the regular fluctuations of η and χ begin. On the other hand, ω decreases rapidly and after 200 fs the regular oscillation starts. The fluctuations are more in case of 298 K than the corresponding 77 K cases as the nuclear kinetic energy is larger in former case than that in the latter. The energy versus time plot is given in Figure 8. As we have started with the crystal structures without optimization of the crystal units, the initial decrease in energy is due to the relaxation of the geometry during simulation. Moreover, after 200 fs we can see the regular fluctuation and oscillation of energy with the increase in time. The intact structure throughout the simulation at 77 K as well as at 298 K indicates the kinetic stability of the **Ne@3a** and **Ne@3b** systems.

6. Conclusions

We have synthesized new porous 3D metal-organic frameworks containing group 2 metals Sr and Ba as infinite chains of planar Sr_n and Ba_n rings. Each metal site in the crystals is coordinated with five protonated nitrilotriacetic acid ligands and

two water molecules. The metal atoms in the crystal carry a positive charge of around 1.0 |e|. The bonding between the metal and oxygen atoms present in the coordination sphere of **3a** and **3b** is of non-covalent type and mostly originating from electrostatic interactions. The computation of interaction energy suggests that one Ne atom can be suitably trapped inside the pores of **3a** and **3b** through an attractive interaction. However, entrapment of other Ng atoms (He, Ar and Kr) are energetically unfavorable. Our *ab initio* molecular dynamics simulations suggest that Ne atom entrapment inside the crystals is kinetically favorable. The optimized geometries show that the Ne atom is situated inside the cavity made by protonated nitrilotriacetic acid ligands and the central metal atom. Since **3a** and **3b** are the smaller representations of the extended crystal structures, therefore it can be assumed that a number of Ne atoms can be accommodated inside the full crystal. The size of the pore inside the crystals is mostly responsible for the observed selectivity of Ne atoms over other noble gases. Therefore, the present crystals could potentially be useful as a filter to separate Ne from a gas mixture.

Acknowledgment

We thank Professor A. I. Boldyrev for helpful discussion and Department of Science & Technology, Government of India, New Delhi for single crystal X-ray and NMR facilities. S.M. and S.P. thank UGC and CSIR, New Delhi respectively for financial assistance. P.K.C. would like to thank DST, New Delhi for the Sir J. C. Bose National Fellowship.

Additional Supporting Information

Additional Supporting Information may be found in the online version of this article.

Figure Captions

Figure 1. ORTEP view of the asymmetric unit of (a) $[Sr(NTA\text{-}H)(H_2O)_{1.5}]$ (b) $[Ba(NTA\text{-}H)(H_2O)_{1.5}]$.

Figure 2. View of the coordination environment of strontium in [Sr(NTA-H)$(H_2O)_{1.5}$]. Color code: Sr; green ball, O; red ball, N; light blue ball, C; gray ball.

Figure 3. View of the bonding mode of the ligand with five strontium ions. Color code: Sr; green ball, O; red ball, N; light blue ball, C; gray ball.

Figure 4. View of the four member Sr_4 ring. Color code: Sr; green ball, O; red ball.

Figure 5. Space fill model of the 3D network viewed along the crystallographic *b* axis. Color code: Sr; green, O; red, N; light blue, C; gray ball.

Figure 6. Geometry of **2a** (shown in a) and **2b** (shown in b). Each metal center surrounded by five NTA-H ligands and 2 water molecules, as a total fourteen NTA-H and six water molecules. Hydrogen atoms are not shown for clarity.

Figure 7. Geometry of **3a** (shown in a) and **3b** (shown in b). Each metal center is nine coordinated. Each metal center is surrounded by five NTA-H ligands and 2 water molecules.

Figure 8. Time (in fs) evolution of energy (in au) for Ne@3a and Ne@3b.

Figures

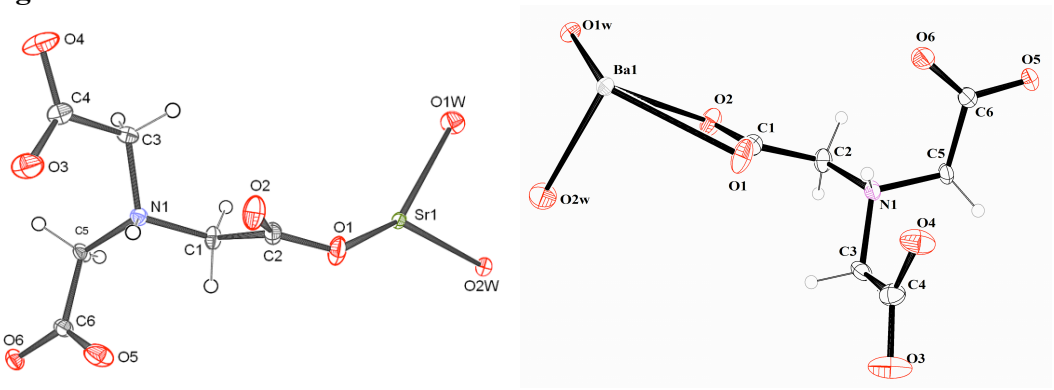

a **b**

Figure 1

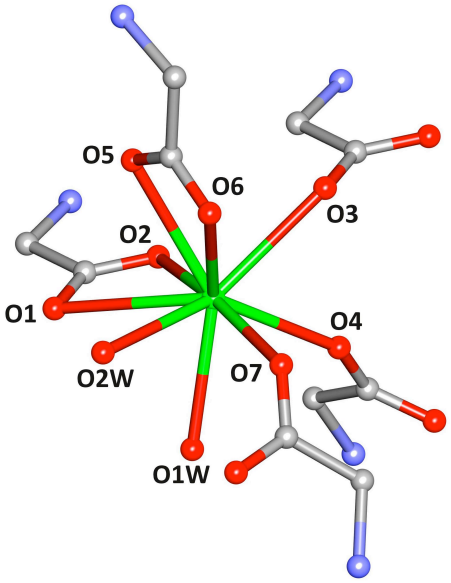

Figure 2

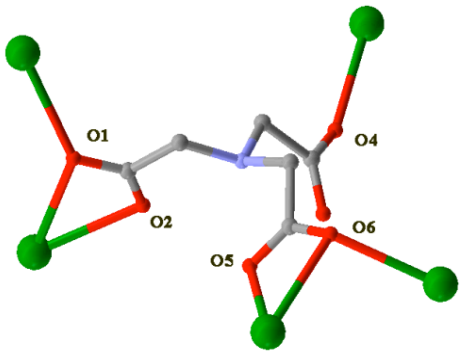

Figure 3

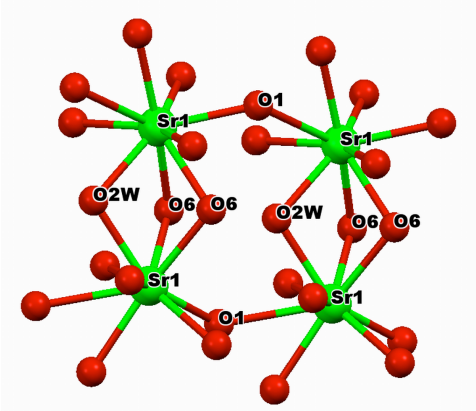

Figure 4

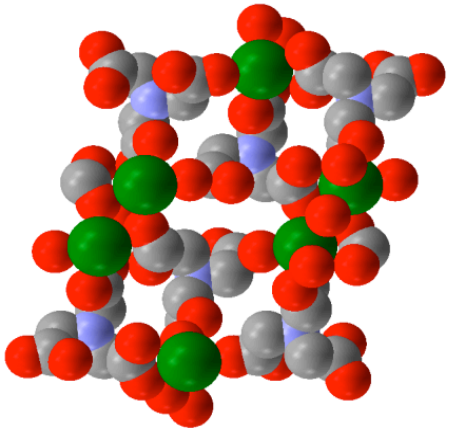

Figure 5

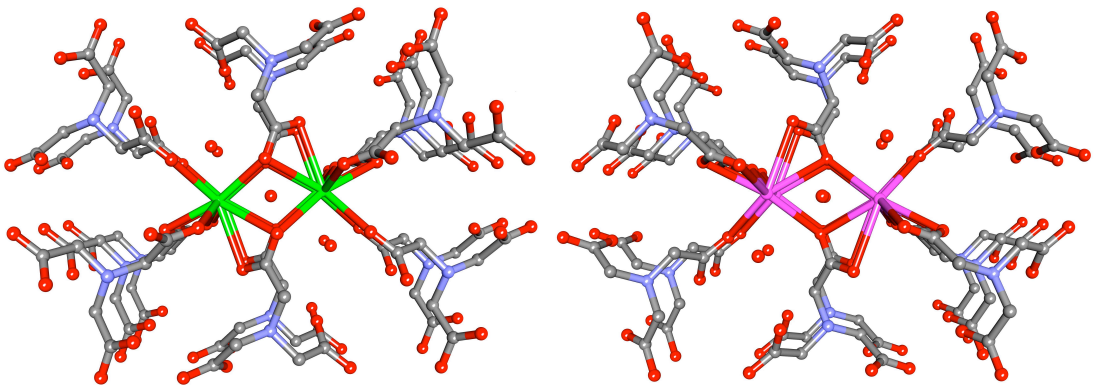

2a **2b**

(a) **(b)**

Figure 6

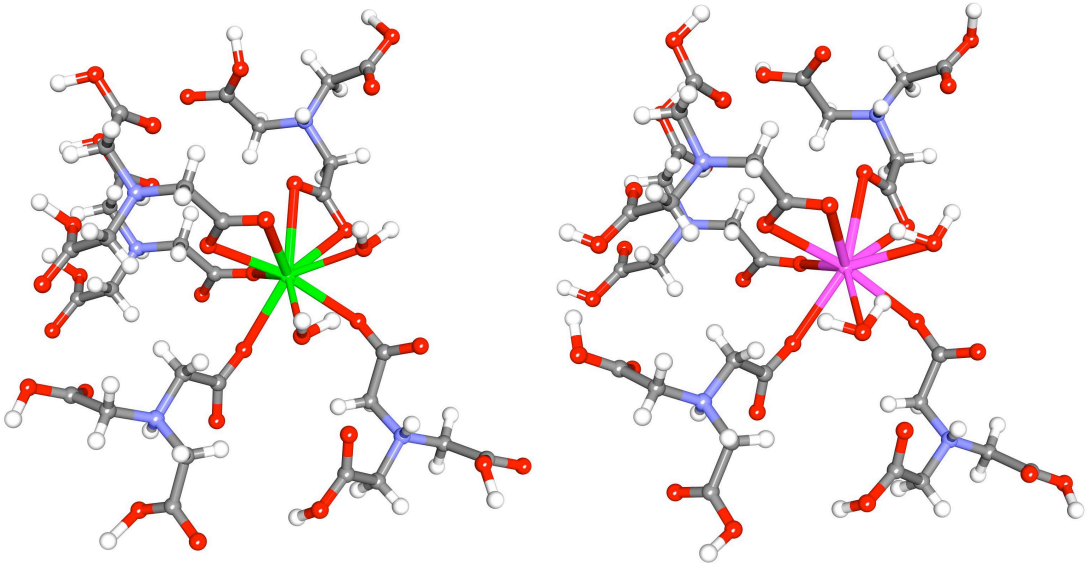

3a **3b**

(a) **(b)**

Figure 7

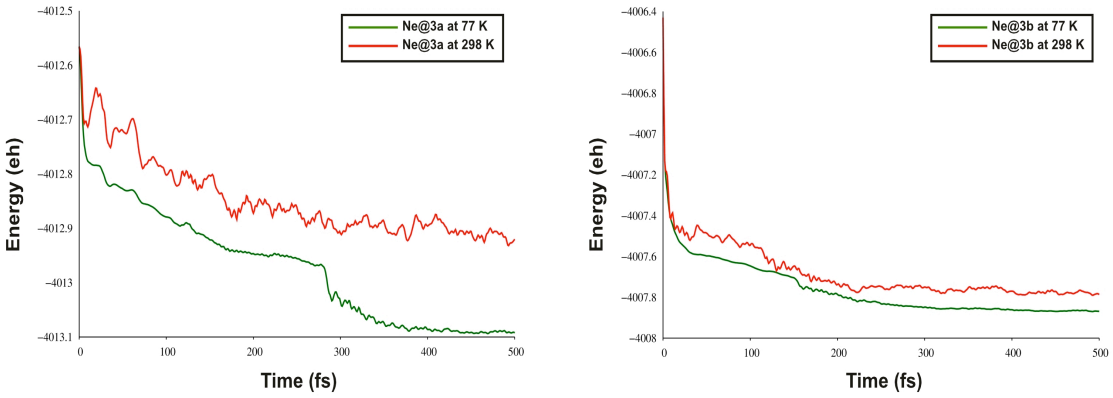

Figure 8

References

[1] A. J. Blake, N. R. Champness, P. Hubberstey, W.-S. Li, M. A. Withersby, M. Schröder, *Coord. Chem. Rev.* **1999**, *183*, 117.
[2] B. Moulton, M. J. Zaworotko, *Chem. Rev.* **2001**, *101*, 1629.
[3] S. L. James, *Chem. Soc. Rev.* **2003**, *32*, 276.
[4] M. Eddaoudi, D. B. Moler, H. Li, B. Chen, T. M. Reineke, M. O'Keeffe, O. M. Yaghi, *Acc. Chem. Res.* **2001**, *34*, 319.
[5] H. Li, M. Eddaudi, M. O'Keeeffe, O. M. Yaghi, *Nature* **1999,** *402*, 276.
[6] (a) R.–Q. Zou, Q. Xu, *Angew Chem. Int. Ed.* **2006**, *45*, 2542; (b) S. Hasegawa, R. Matsuda, S. Furukawa, M. Katsunori, S. Kitagawa, *J. Am. Chem. Soc.* **2007**, *129*, 2607; (c) M. Higuchi, D. Tanaka, S. Horike, H. Sakamoto, K. Nakamura, Y. Takashima, Y. Hijikata, N. Yanai, J. Kim, K. Kato, Y. Kubota, M. Takata, S. Kitagawa, *J. Am. Chem. Soc*. **2009**, *131*, 10336; (d) S. S.–Y. Chui, S. M.–F. Lo, J. P. H. Charmant, A. G. Orpen, I. D. Williams, *Science* **1999**, *283*, 1148; (e) B. Li, H.-M. Wen, W. Zhou, B. Chen, *J. Phys. Chem. Lett.* **2014**, *5*, 3468.
[7] A. Mavrandonakis, E. Klontzas, E. Tylianakis, G. E. Froudakis, *J. Am. Chem. Soc.* **2009**, *131,* 13410.
[8] J. L. C. Rowsell, O. M. Yaghi, *J. Am. Chem. Soc.* **2006**, *128,* 1304.
[9] J. L. C. Rowsell, A. R Millward, K. S. Park, O. M. Yaghi, *J. Am. Chem. Soc.* **2004**, *126,* 5666.
[10] B. Chen, C. Liang, J. Yang, D. S. Contreras, Y. L. Clancy, E. B. Lobkovsky, O. M. Yaghi, S. Dai, *Angew Chem. Int. Ed.* **2006**, *45*, 1390.
[11] D. Britt, D. Tranchemontagne, O. M. Yaghi, *PNAS* **2008**, *105,* 11623.
[12] (a) C. A. Williams, A. J. Blake, C. Wilson, P. Hubberstey, M. Schröder, *Crystal Growth & Design* **2008**, *8,* 911; (b) M. Dincâ, J. R. Long, *J. Am. Chem. Soc.* **2005**, *127*, 9376; (c) I. Senkovska, S. Kaskel, *Eur. J. Inorg. Chem.* **2006**, *2006*, 4564; (d) J. A. Rood, B. C. Noll, K. W. Henderson, *Inorg. Chem.* **2006**, *45*, 5521.
[13] S. Ma, H.-C. Zhou, *Chem. Commun.* **2010**, *46*, 44.
[14] (a) L. Khriachtchev, M. Pettersson, J. Lundell, H. Tanskanen, T. Kiviniemi, N. Runeberg, M. Räsänen, *J. Am. Chem. Soc*. **2003**, *125*, 1454; (b) L. Khriachtchev, H. Tanskanen, A. Cohen, R. B. Gerber, J. Lundell, M. Pettersson, H. Kiljunen, M. Räsänen, *J. Am. Chem. Soc*. **2003** *125*, 6876; (c) H. Tanskanen, L. Khriachtchev, J. Lundell, H. Kiljunen, M. Räsänen, *J. Am. Chem. Soc*. **2003**, *125*, 16361.
[15] (a) V. I. Feldman, F. F. Sukhov, A. Yu. Orlov, I. V. Tyulpina, *J. Am. Chem. Soc*. **2003**, *125*, 4698; (b) V. I. Feldman, A.V. Kobzarenko, I. A. Baranova, A. V. Danchenko, F. F. Sukhov, E. Tsivion, R. B. Gerber, *J. Chem. Phys*. **2009**, *131*, 151101; (c) S. V. Ryazantsev, A. V. Kobzarenko, V. I. Feldman, *J. Chem. Phys*. **2013**, *139*, 124315.
[16] (a) J. Li, B. E. Bursten, B. Liang, L. Andrews, *Science* **2002**, *295*, 2242; (b) B. Liang, L. Andrews, J. Li, B. E. Bursten, *J. Am. Chem. Soc.* **2002**, *124*, 9016; (c) X. Wang, L. Andrews, J. Li, B. E. Bursten, *Angew. Chem. Int. Ed.* **2004**, *43*, 2554.
[17] (a) S. A. Cooke, M. C. L. Gerry, *Phys. Chem. Chem. Phys*. **2004**, *6*, 3248; (b) S. A. Cooke, M. C. L. Gerry, *J. Am. Chem. Soc*. **2004**, *126*, 17000; (c) J. M. Michaud, M. C. L. Gerry, *J. Am. Chem. Soc*. **2006**, *128*, 7613.
[18] (a) G. L. Smith, H. P. A. Mercier, G. J. Schrobilgen, *Inorg. Chem.* **2011**, *49*, 12359; (b) D. S. Brock, H. P. A. Mercier, G. J. Schrobilgen, *J. Am. Chem. Soc.* **2013**,

135, 5089; (c) J. R. Debackere, H. P. A. Mercier, G. J. Schrobilgen, *J. Am. Chem. Soc.* **2014**, *136*, 3888.
[19] (a) C. Ó. Jiménez-Halla, I. Fernández, G. Frenking, *Angew. Chem. Int. Ed*. **2009**, *48*, 366; (b) L. A. Mück, A. Y. Timoshkin, M. v. Hopffgarten, G. Frenking, *J. Am. Chem. Soc*. **2009**, *131*, 3942; (c) I. Fernández, G. Frenking, *Phys. Chem. Chem. Phys*. **2012**, *14*, 14869; (d) Q. Zhang, M. Chen, M. Zhou, D. M. Andrada, G. Frenking, *J. Phys. Chem. A* **2015**, *119*, 2543.
[20] (a) D. Kurzydłowski, P. Ejgierd-Zaleski, W. Grochala, R. Hoffmann, *Inorg. Chem*. **2011**, *50*, 3832; (b) W. Grochala, *Phys. Chem. Chem. Phys*. **2012**, *14*, 14860; (c) P. Szarek, W. Grochala, *J. Phys. Chem. A* **2015**, *119*, 2483.
[21] (a) P. Antoniotti, E. Bottizzo, L. Operti, R. Rabezzana, S. Borocci, F. Grandinetti, *J. Phys. Chem. Lett*. **2010**, *1*, 2006; (b) L. Operti, R. Rabezzana, F. Turco, S. Borocci, M. Giordani, F. Grandinetti, *Chem. Eur. J*. **2011**, *17*, 10682; (c) S. Borocci, M. Giordani, F. Grandinetti, *J. Phys. Chem. A* **2015**, *119*, 2383.
[22] (a) A. Sirohiwal, D. Manna, A. Ghosh, T. Jayasekharan, T. K. Ghanty, *J. Phys. Chem*. *A* **2013**, *117*, 10772; (b) D. Manna, A. Ghosh, T. K. Ghanty, *J. Phys. Chem*. *A* **2013**, *117*, 14282; (c) A. Ghosh, D. Manna, T. K. Ghanty, *J. Phys. Chem*. *A*, **2015** *119*, 2233.
[23] (a) S. Pan, M. Contreras, J. Romero, A. Reyes, P. K. Chattaraj, G. Merino, *Chem. Eur. J*. **2013**, *19*, 2322; (b) S. Pan, S. Jalife, R. M. Kumar, V. Subramanian, G. Merino, P. K. Chattaraj, *ChemPhysChem* **2013**, *14*, 2511; (c) S. Pan, S. Jalife, J. Romero, A. Reyes, G. Merino, P. K. Chattaraj, *Comput. Theor. Chem*. **2013**, *1021*, 62; (d) S. Pan, D. Moreno, J. L. Cabellos, J. Romero, A. Reyes, G. Merino, P. K. Chattaraj, *J. Phys. Chem. A* **2014**, *118*, 487; (e) S. Pan, D. Moreno, J. L. Cabellos, G. Merino, P. K. Chattaraj, *ChemPhysChem* **2014**, *15*, 2618; (f) S. Pan, D. Moreno, G. Merino, P. K. Chattaraj, *ChemPhysChem* **2014**, *15*, 3554; (g) S. Pan, R. Saha, P. K. Chattaraj, *Int. J. Mol. Sci*. **2015**, *16*, 6402; (h) R. Saha, S. Pan, P. K. Chattaraj, *J. Phys. Chem. A* **2015**, DOI: 10.1021/acs.jpca.5b03888.
[24] (a) M. Saunders, H. A. Jiménez-Vázquez, R. J. Cross, R. J. Poreda, *Science* **1993**, *259*, 1428; (b) M. Saunders, R. J. Cross, H. A. Jiménez-Vázquez, R. Shimshi, A. Khong, *Science* **1996***, 271,* 1693*;* (c) M. Saunders, H. A. Jiménez-Vázquez, R. J. Cross, *J. Am. Chem. Soc.* **1994,** *116***,** 2193; (d) H. A. Jiménez-Vázquez, R. J. Cross, *J. Chem. Phys.* **1996**, *104*, 5589; (e) M. S. Syamala, R. J. Cross, M. Saunders, *J. Am. Chem. Soc.* **2002**, *124*, 6216; (f) K. Yamamoto, M. Saunders, A. Khong, R. J. Cross, Jr., Michael Grayson, M. L. Gross, A. F. Benedetto, R. B. Weisman, *J. Am. Chem. Soc.* **1999**, *121*, 1591; (g) M. Murata, Y. Murata, K. Komatsu, *Chem. Commun.* **2008**, 6083.
[25] (a) A. Krapp, G. Frenking, *Chem. Eur. J.* **2007**, *13*, 8256; (b) S. Osuna, M. Swart, M. Solà, *Chem. Eur. J.* **2009**, *15*, 13111; (c) M. Bühl, S. Patchkovskii, W. Thiel, *Chem. Phys. Lett.* **1997**, *275,* 14; (d) M. Khatua, S. Pan, P. K. Chattaraj, *J. Chem. Phys.* **2014**, *140*, 164306; (e) M. Khatua, S. Pan, P. K. Chattaraj, *Chem. Phys. Lett.* **2014**, *610–611*, 351; (f) S. Pan, S. Mandal, P. K. Chattaraj, *J. Phys. Chem. B* **2015**, DOI: 10.1021/acs.jpcb.5b01396.
[26] (a) J. A. Greathouse, T. L. Kinnibrugh, M. D. Allendorf, *Ind. Eng. Chem. Res.* **2009**, *48*, 3425; (b) M. V. Parkes, C. L. Staiger, J. J. Perry IV, M. D. Allendorfc, J. A. Greathouse, *Phys.Chem. Chem. Phys.* **2013**, *15*, 9093.
[27] P. Ryan, O. K. Farha, L. J. Broadbelt, R. Q. Snurr, *AIChE J*. **2011**, *57*, 1759.
[28] Y. Gurdal, S. Keskin, *Ind. Eng. Chem. Res.* **2012**, *51*, 7373.
[29] Crystal data are supplied as CIF files along with the supporting information file.

[30] L. J. Farrugia**,** *J. Appl. Crystallogr.* **1999**, *32*, 837**.**
[31] G. M. Sheldrick, *Acta Crystallogr., Sect. A* **2008**, *A64*, 112.
[32] L. J. Farrugia, *J. Appl. Crystallogr.* **2012**, *45*, 849.
[33] Gaussian 09, (*Revision C.01*), Gaussian Inc., Wallingford CT, **2010**.
[34] (a) A. D. Becke, *J. Chem. Phys.* **1993**, *98*, 5648; (b) C. Lee, W. Yang, R. G. Parr, *Phys. Rev. B* **1988**, *37*, 785.
[35] (a) R. Ditchfield, W. J. Hehre, J. A. Pople, *J. Chem. Phys.* **1971**, *54*, 724; (b) W. J. Hehre, R. Ditchfield, J. A. Pople, *J. Chem. Phys.* **1972**, *56*, 2257.
[36] F. Weigend, R. Ahlrichs, *Phys. Chem. Chem. Phys.* **2005**, *7*, 3297.
[37] M. Kaupp, P. v. R. Schleyer, H. Stoll, H. Preuss, *J. Chem. Phys.* **1991**, *94*, 1360.
[38] A. E. Reed, F. Weinhold, *J. Chem. Phys.***1983**, *78*, 4066.
[39] T. Lu, F. W. Chen, *J. Comput. Chem*. **2012**, *33*, 580.
[40] R. G. Parr, R. A. Donnelly, M. Levy, W. E. Palke, *J. Chem. Phys.* **1978**, *68*, 3801.
[41] (a) R. G. Pearson, *Chemical Hardness: Applications from Molecules to Solids*; Wiley-VCH: Weinheim, Germany, **1997;** (b) R. G. Parr, R. G. Pearson, *J. Am. Chem. Soc.* **1983**, *105*, 7512; (c) R. G. Parr, P. K. Chattaraj, *J. Am. Chem. Soc*. **1991**, *113*, 1854; (d) S. Pan, M. Solà, P. K. Chattaraj, *J. Phys. Chem. A* **2013**, *117*, 1843.
[42] (a) R. G. Parr, L. v. Szentpály, S. Liu, *J. Am. Chem. Soc.* **1999**, *121*, 1922; (b) P. K. Chattaraj, S. Giri, S. Duley, *Chem. Rev.* **2011**, *111*, PR43.
[43] T. A. Koopmans, *Physica* **1933**, *1*, 104.
[44] (a) R. Ahlrichs, M. Bar, M. Haser, H. Horn, C. Kolmel, *Chem. Phys. Lett.* **1989**, *162*, 165; (b) TURBOMOLE, V6.5: A development of University of Karlsruhe and Forschungszentrum Karlsruhe GmbH, 1989–2007; TURBOMOLE GmbH: Karlsruhe, Germany, since 2007, **2013**.
[45] K. Eichkorn, F. Weigend, O. Treutler, R. Ahlrichs, *Theor. Chem. Acc.* **1997**, *97*, 119.
[46] S. Grimme, J. Antony, S. Ehrlich, H. Krieg, *J. Chem. Phys.* **2010**, *132*, 154104.
[47] S. Grimme, S. Ehrlich, L. Goerigk, *J. Comput. Chem.* **2011**, *32*, 1456.
[48] (a) H. B. Schlegel, J. M. Millam, S. S. Iyengar, G. A. Voth, A. D. Daniels, G. E. Scuseria, M. J. Frisch, *J. Chem. Phys.* **2001**, *114*, 9758; (b) S. S. Iyengar, H. B. Schlegel, J. M. Millam, G. A. Voth, G. E. Scuseria, M. J. Frisch, *J. Chem. Phys.* **2001**, *115*, 10291; (c) H. B. Schlegel, S. S. Iyengar, X. Li, J. M. Millam, G. A. Voth, G. E. Scuseria, M. J. Frisch, *J. Chem. Phys.* **2002**, *117*, 8694.
[49] B. L. Barnett, V. A. Uchtman, *Inorg. Chem*. **1979***, 18*, 2674.
[50] X.-Q. Lu, J.-J. Jiang, C.-L. Chen, B.-S. Kang, C.-Y. Su, *Inorg. Chem*. **2005**, *44*, 4515.
[51] K. B. Wiberg, *Tetrahedron* **1968**, *24*, 1083.
[52] R. F. W. Bader, *Atoms in molecules: A quantum theory*; Clarendon press: Oxford, UK, **1990**.
[53] P. Macchi, L. Garlaschelli, S. Martinengo, A. Sironi, *J. Am. Chem. Soc*. **1999**, *121*, 10428.
[54] (a) J. Cioslowski, S. T. Mixon, *Can. J. Chem*. **1992**, *70*, 443; (b) J. Cioslowski, S. T. Mixon, *J. Am. Chem. Soc*. **1992**, *114*, 4382.
[55] S. Pan, A. Gupta, S. Mandal, D. Moreno, G. Merino, P. K. Chattaraj, *Phys. Chem. Chem. Phys*. **2015**, *17*, 972.
[56] D. Cremer, E. Kraka, *Angew. Chem*. **1984**, *96*, 612; *Angew. Chem. Int. Ed. Engl*. **1984**, *23*, 627.

[57] M. Ziolkowski, S. J. Grabowski, J. Leszczynski, *J. Phys. Chem. A* **2006**, *110*, 6514.
[58] P. Macchi, D. M. Proserpio, A. Sironi, *J. Am. Chem. Soc*. **1998**, *120*, 13429.
[59] I. V. Novozhilova, A, V. Volkov, P. Coppens, *J. Am. Chem. Soc*. **2003**, *125*, 1079.
[60] (a) W. Wang, D. Yuan, *Sci. Rep.* **2014**, *4,* 5711; (b) Y. Li1, T. Ben, B. Zhang1, Y. Fu, S. Qiu, *Sci. Rep.* **2013**, *3*, 2420; (c) S. Gadipelli, Z. X. Guo, *Prog. Mater. Sci.* **2015**, *69*, 1; (d) Y. Basdogana, S. Keskin, *Cryst. Eng. Comm.* **2015**, *17*, 261.